Journal of Zhejiang University-SCIENCE B (Biomedicine & Biotechnology) *2021 22(12):1022-1033*
www.jzus.zju.edu.cn; www.springer.com/journal/11585
E-mail: jzus_b@zju.edu.cn

Research Article
https://doi.org/10.1631/jzus.B2100644

3D printing of bioinspired compartmentalized capsular structure for controlled drug release

Jingwen LI[1*], Mingxin WU[2*], Wenhui CHEN[1], Haiyang LIU[1], Di TAN[1], Shengnan SHEN[1✉], Yifeng LEI[2✉], Longjian XUE

[1]*School of Power and Mechanical Engineering, Wuhan University, Wuhan 430072, China*
[2]*The Institute of Technological Science, Wuhan University, Wuhan 430072, China*

Abstract: Drug delivery with customized combinations of drugs, controllable drug dosage, and on-demand release kinetics is critical for personalized medicine. In this study, inspired by successive opening of layered structures and compartmentalized structures in plants, we designed a multiple compartmentalized capsular structure for controlled drug delivery. The structure was designed as a series of compartments, defined by the gradient thickness of their external walls and internal divisions. Based on the careful choice and optimization of bioinks composed of gelatin, starch, and alginate, the capsular structures were successfully manufactured by fused deposition modeling three-dimensional (3D) printing. The capsules showed fusion and firm contact between printed layers, forming complete structures without significant defects on the external walls and internal joints. Internal cavities with different volumes were achieved for different drug loading as designed. In vitro swelling demonstrated a successive dissolving and opening of external walls of different capsule compartments, allowing successive drug pulses from the capsules, resulting in the sustained release for about 410 min. The drug release was significantly prolonged compared to a single burst release from a traditional capsular design. The bioinspired design and manufacture of multiple compartmentalized capsules enable customized drug release in a controllable fashion with combinations of different drugs, drug doses, and release kinetics, and have potential for use in personalized medicine.

Key words: Three-dimensional (3D) printing; Bioinspired; Capsule; Bioink; Drug release

1 Introduction

Drug delivery with customized adaptation of the active ingredients, controllable dosage and strength, on-demand release kinetics, and administration mode is critical for personalized medicine (Jameson and Longo, 2015). Great effort has been devoted to devising novel solutions to achieve better drug delivery to patients in need. However, the improvement of drug delivery has not kept up with the growing demands of patients. For example, a patient with cancer may need different drug formulations as tablets, powder, capsules, or injections several times a day. Therefore, the design of advanced therapeutic systems that provide versatile combinations of drugs, drug doses, and drug release kinetics is desirable. Sustained drug release formulations have attracted great attention in pharmaceutical fields, due to their significant advantages such as maintaining a stable and effective drug concentration, prolonging efficacy, reducing the number of drugs used, reducing toxic and side effects, and reducing the total dose of drug used (Norman et al., 2017; Lim et al., 2018).

In nature, successive opening of multilayered structures of flowers (such as rose or lotus) enables a sustained release of floral aroma. These natural structures inspired us to design a biomimetic structure for controlled drug delivery. However, these natural structures generally have complex geometry, and are therefore difficult to fabricate by traditional manufacturing methods. To this end, additive manufacturing (namely three-dimensional (3D) printing) provides advantages over traditional manufacturing approaches, such as

✉ Yifeng LEI, yifenglei@whu.edu.cn
Shengnan SHEN, Shen_Shengnan@whu.edu.cn
* The two authors contributed equally to this work
Yifeng LEI, https://orcid.org/0000-0002-3523-6887
Shengnan SHEN, https://orcid.org/0000-0002-3964-8475

Received May 31, 2021; Revision accepted July 20, 2021;
Crosschecked Nov. 18, 2021

fabrication with high tunability and complexity (Ligon et al., 2017; Bose et al., 2018). In particular, 3D bioprinting is an extended application of 3D printing for printing biocompatible and functional materials in layer-by-layer structures (Ozbolat et al., 2016; Peng et al., 2019; Zhang et al., 2019). It has been widely used in biological and biomedical applications (Liaw and Guvendiren, 2017; Zhu et al., 2021), such as tissue engineering and regenerative medicine (Holland et al., 2018; Zhang et al., 2019; Lawlor et al., 2021), stem cell differentiation (An et al., 2020), disease models (Li et al., 2020; Maharjan et al., 2021), and organ repair (Noor et al., 2019; Urciuolo et al., 2020), and in drug delivery fields (Trivedi et al., 2018; Chen et al., 2020).

3D printing has been exploited to achieve personalization of drug products based on digital design and manufacturing (Gioumouxouzis et al., 2019), where the dose regimes and the dosage forms can be easily customized during printing. A wide range of materials, multiscale geometries, and multi-functional structures have been designed to efficiently control drug-release profiles (Zhang et al., 2017). 3D-printed drug delivery devices have been previously demonstrated for controlled and tunable drug release. These devices include tablets with holes of variable size (Lim et al., 2016), honeycomb architecture tablets (Kyobula et al., 2017), tablets with infill patterns (Kadry et al., 2018), gastro-floating tablets (Li et al., 2018), radiator-like capsules (Isreb et al., 2019), bilayer tablets (Fina et al., 2018), cylindrical capsules (Maroni et al., 2017), layered-architectures of polypills (Pereira et al., 2019), and microneedle drug delivery systems (Wu et al., 2020; Economidou et al., 2021). However, the design, manufacturing process, and drug release behavior of more complex bioinspired structures have rarely been reported.

To this end, in this study, inspired by natural plant structures, we aimed to design a multiple compartmentalized capsule structure for controlled drug delivery. We used fused deposition modeling (FDM) 3D printing to manufacture the capsular delivery devices, and demonstrated their ability for controlled drug release.

2 Materials and methods

2.1 Materials

Gelatin from porcine skin, starch from rice, and sodium alginate (SA) were obtained from Sigma-Aldrich (Shanghai, China). The materials were of reagent grade and were used as received without further purification. Doxorubicin hydrochloride (DXR) was purchased from Sinopharm Chemical Reagent (Shanghai, China). Different colored dyes were obtained from Marie's Water Color (Beijing, China). Saline was purchased from Thermo-Fisher Scientific (Shanghai, China). Milli-Q water with a resistivity of 18 MΩ served as a general solvent during the fabrication.

2.2 Design of biomimetic sustained-release capsules

Inspired by successive opening of flowers which gives sustained fragrance release (Fig. 1a), the original design for the controlled drug release device was a multilayered structure in which the successive opening of multilayers of capsules could provide a sustained release of encapsulated drugs. However, these multilayered structures were difficult to print due to their complex geometries (Velasco-Hogan et al., 2018). Further, inspired by natural plant tissues consisting of multiple compartmentalized structures containing seed or fruit in chambers (Fig. 1b), we designed a compartmentalized capsular structure with several chambers with different wall thickness (Fig. 1c). By doing this, the successive opening of different chambers to achieve a sustained drug release could mimic the successive opening of multilayers of flowers (Fig. 1d).

An enclosed structure with a cubic, rectangular, cylindrical, or spherical shape is difficult to manufacture using a 3D printing process, because the internal cavity

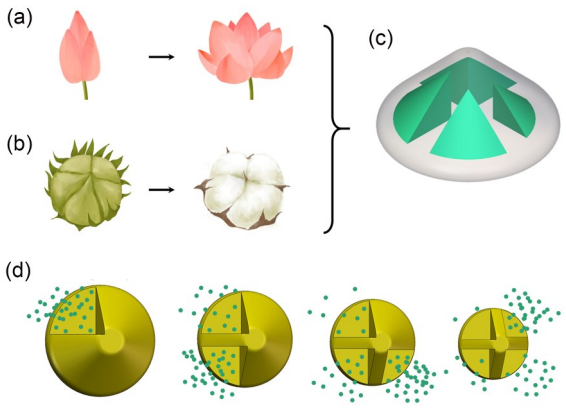

Fig. 1 Schematic design of a multi-bioinspired capsular structure for controlled drug release. (a) Successive opening of multilayers of flowers enables sustained fragrance release; (b) Multiple compartmentalized structure of cotton; (c, d) Scheme (c) and successive opening (d) of a compartmentalized structure for controlled drug release.

can promote the collapse of suspended structures. To address this problem, we designed a tapered capsular structure (Fig. 2a), and a circular arc was designed for the top surface to increase the compliance for application in vivo (Figs. 2a and 2b). The capsule consisted of a base and an elliptical dome containing four compartments (Figs. 2b and 2c), in which different drugs and dosages could be loaded.

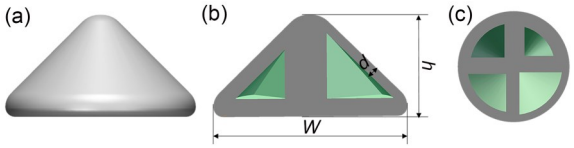

Fig. 2 Structural design of a multiple compartmentalized capsule. (a) Front view; (b) Vertical section view; (c) Horizonal section view.

The four compartments of capsules were defined by the thickness of their external walls, and further separated by internal divisions (Fig. 2c). The base width, height, and thicknesses of external walls and internal joints were variable parameters (Table 1). The thickness of the internal joints was set as the sum of the thickness of two adjacent external walls, and the thickness of the base was equal to that of the largest internal joints. For capsules as controls, the external walls of each compartment were the same. The capsular structures were designed using Solidworks software (Version 2016, Dassault Systèmes, USA). STL format files were saved and exported for 3D printing.

2.3 Preparation of bioinks for 3D printing

We used biocompatible materials that are currently used in the pharmaceutical industry, including gelatin, starch, and SA, to prepare different formulations of bioinks for 3D printing. Gelatin (0%–20% (1%=0.01 g/mL, the same below)) was mixed in water and heated to 50 °C for complete dissolution. Next, different concentrations of starch (0%–10%) were added to the gelatin solution and mixed under rigorous agitation. Different concentrations of SA (0%–25%) were then added to the gelatin-starch mixture. The obtained bioinks were stored at 4 °C, at which temperature the bioinks were in a gel state due mainly to the gelatin component (Bohidar and Jena, 1993). The stored bioinks were heated to above 45 °C to become sol state for 3D printing use.

2.4 Rheological characterization of bioinks

The rheological properties of the bioinks were characterized using a rheometer (Anton Paar MCR92, Graz, Austria). To measure their viscosity, the bioinks were loaded with steady rate sweeps with a shear rate of 0–500 s^{-1}. To measure the shear modulus (including storage modulus (G') and loss modulus (G")) of the bioinks, frequency sweep tests were used from 0.1 to 100 rad/s at a constant strain of 1% in the linear viscoelastic region. The viscosity was measured at 45 °C, whereas the shear modulus measurement was carried out at room temperature.

2.5 Printing of capsular devices

We used a desktop bioprinter (Allevi 2, Philadelphia, USA) to carry out 3D printing of capsular structures with the above design. The bioprinter contained two separate extruder systems (Fig. 3a), which could be loaded with different bioinks and work independently. Herein, we used one extruder to print the capsule structure as designed, and the other to print the drug-containing formulations.

The above bioinks were dispensed in an extrusion system, and the container was heated to 45 °C to increase their fluidity (Fig. 3b). The nozzle tip (0.41 mm in diameter) was set at 35 °C (Fig. 3b), and the deposition platform was set at room temperature. The pressure of the nozzles was adjusted to 1.9–2.2 bar (1 bar= 100 kPa) until the bioink was extruded and the filament was stabilized without breaking. Then, the nozzle tip was brought down to touch the platform, and the printing process started.

The printing speed was set at 10 mm/s, the printing layer thickness was 400 μm, and the solid fill was 100%. The capsular structure was printed layer-by-layer by the moving system, and the printing time for a capsule device with a base diameter of 20 mm and a height of 8 mm was about 13–14 min. Different

Table 1 Parameter setting of compartmentalized capsules

Group	Base diameter (mm)	Height (mm)	External wall thickness (mm)				Maximum storage capacity (mm^3)
			Chamber 1	Chamber 2	Chamber 3	Chamber 4	
Capsule 1	15.00	8.00	1.15	1.40	1.65	1.90	33.84
Capsule 2	20.00	8.00	1.15	1.40	1.65	1.90	192.84

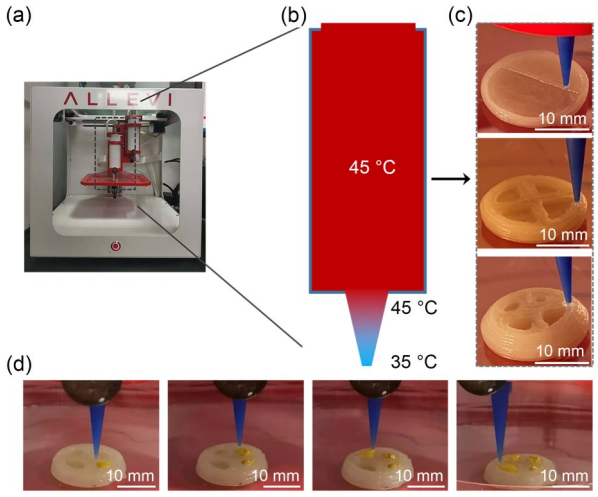

Fig. 3 3D printing of compartmentalized capsular structures. (a) Image of the 3D printer with two separate extrusion systems; (b) Illustration of the temperature setting of the bioink container and extrusion nozzle; (c) Images of the printing process of the base, middle, and top parts of the capsule; (d) Images of drug loading into different compartments of the capsular structure. 3D, three-dimensional.

physical forms of drug formulations such as solids and liquids could be loaded into different chambers of the capsules using the second extruder system of the printer (Fig. 3a), by adjusting the nozzle output velocity and droplet size of the drug solutions. Subsequently, the printed capsules were air-dried at room temperature for one day (Li et al., 2019), then stored in a cool and dry environment for experimental use.

2.6 Characterization of printed structures

The morphology, print accuracy, and defects of the capsular structures were characterized by digital photographs, scanning electron microscopy (SEM; TESCAN Mira3, Brno-Kohoutovice, Czech Republic) and micro-computed tomography (micro-CT; Skyscan 1176, Kontich, Belgium), respectively. The porosity in the printed structure was calculated from SEM images using ImageJ software (National Institutes of Health (NIH), USA). The thicknesses of external walls and internal divisions were measured from cross-sectional computed tomography (CT) images using ImageJ software.

2.7 In vitro swelling assay

For demonstration of drug release in vitro, different colored dyes were loaded into each compartment of the capsule (20 mm in base diameter, 8 mm in height). Each compartment was loaded with 10 mg of liquid formulations with different colored dyes, including black, white, violet, and orange. The capsules were put on a shelf and immersed in 20 mL saline solution under mild agitation (100 r/min) at 37 °C. The appearance of the capsules was observed by digital photographs after different incubation time.

2.8 In vitro drug release evaluation

For in vitro drug release, a fluorescence drug, DXR, was loaded into the capsules for interpretation. Each compartment of the capsule was loaded with 5 mg DXR. The capsules (n=3 for each group) were incubated in 15 mL saline under mild agitation as described above. At different time points, 20 μL of the supernatant was collected and centrifuged, and the fluorescence intensity of DXR in the supernatant was measured using a fluorescence spectrophotometer (Agilent Cary Eclipse, Palo Alto, USA), with excitation at 485 nm and emission at 595 nm. The concentration of released DXR was calculated with a calibration curve with a series of predetermined DXR dilutions. Then the cumulative drug release profile was plotted as a function of incubation time.

The following parameters were analyzed according to the drug release profile: time to 5% release ($t_{5\%}$), which indicated the start of drug release; time to 95% release ($t_{95\%}$), which represented almost complete drug release; time interval to achieve complete release ($t_{95\%-5\%}$), which defined the duration of drug release.

3 Results and discussion

3.1 Design of capsular devices

Inspired by the successive opening of flowers and multiple compartmentalized structures of plants, we designed a compartmentalized capsular device for controlled drug release (Figs. 1a–1c), in which the successive opening of different compartments mimics the sustained release behavior of plants (Fig. 1d).

The capsular structure was designed in the form of four hollow compartments, each consisting of a quarter of a cone with increasing volume (Fig. 2). The designed compartments are separated by internal divisions in the middle which act as partition walls as well as internal joints (Fig. 2). The external walls and internal divisions of the compartments differ in thickness (Figs. 2b and 2c), and compartments with thicker external walls have smaller internal cavities (Fig. 2c).

Moreover, the external walls vary in a series of increasing thickness (Fig. 2c and Table 1). With this design, the successive opening of the external walls with a thickness gradient enables a sustained drug release from the structure.

3.2 Bioink optimization and printability

We used pharmaceutical-grade polymers, including gelatin, starch, and SA to prepare bioinks for 3D printing. The choice of materials for 3D printing of the capsules was based on the consideration of biocompatibility, printability, degradation, and release profiles of the capsular structure (Ligon et al., 2017; Velasco-Hogan et al., 2018; Zhu et al., 2021). Gelatin was used as the basic material of the capsular device due to its biocompatibility, its application in food and pharmaceutical industries, and more specifically its thermoreversible gelation ability (Bohidar and Jena, 1993; You et al., 2020). Gelatin can be dissolved to form an aqueous solution above the body temperature of 37 °C, and goes through a sol–gel transition upon cooling to room temperature or lower (Duconseille et al., 2015). The advantage of the sol–gel transition of gelatin is that the shape fidelity of the 3D-printed structure can be regulated by temperature control. Starch is also a popular food ingredient which can be dissolved in solution (Elvira et al., 2002). Gelatin-starch blends have been widely used as capsule materials in the pharmaceutical industry (Zhang et al., 2013). Based on preliminary experiments (data not shown), we used 20% gelatin and 10% starch blends to form basic bioinks. However, the obtained gelatin-starch bioinks showed high fluidity at high temperatures, and extrusion to form filaments during printing proved difficult (Fig. S1a), even at cooler temperatures.

To solve this problem, we added SA to the gelatin-starch blend to improve its rheological properties as well as the printability of the bioink (Paxton et al., 2017). Alginate has excellent biocompatibility, regulable viscosity, and ionotropic gelation property, and allows for fabrication of complex structures (Lee and Mooney, 2012; Rastogi and Kandasubramanian, 2019). Different concentrations of SA were added to the gelatin-starch blend, and the rheological properties of the bioinks were investigated, including shear-thinning and rapid-gelling properties, which are key requirements for extrusion-based 3D printing (Ozbolat and Hospodiuk, 2016; Placone and Engler, 2018). The viscosity of the gelatin/starch/SA bioinks was much higher than that of the gelatin-starch blend (Fig. 4a), and the higher the SA concentration, the higher the viscosity (Figs. 4a and 4b). Moreover, the bioinks exhibited a shear-thinning behavior with increasing shear rates (Fig. 4a). Therefore, the bioink could be easily extruded from the nozzle (Guvendiren et al., 2012), after which it formed stable filaments because of the release of shear stress. Moreover, the storage modulus (G') of the gelatin/starch/SA bioinks was higher than the loss modulus (G") at room temperature (Fig. 4c). This indicated that the printed product had a gelled structure after deposition, thereby facilitating the shape fidelity of the printed structures on the platform preset at room temperature.

With addition of 1%–10% SA to the bioink, the printed structures collapsed after the deposition process (Figs. 4d, S1a–S1c, and S2a–S2c) due to the high fluidity of the bioinks. With a higher amount of SA (25%) in the bioink, it was hardly extruded from the nozzle (Fig. S1f), and the printed layers showed poor adhesion (Fig. S2f), resulting in poor shape fidelity of the printed structure (Figs. 4d and S2f). Bioinks with addition of 15%–20% SA showed a proper viscosity and shear-thinning property for printing (Fig. 4a). The bioink extruded from the nozzle formed a good filament (Figs. S1d and S1e), and the deposited structure showed good shape fidelity with good adhesion among the printed layers (Figs. 4d and S2d–S2f). However, after the drying process, the structure printed with bioink containing 15% SA underwent much more significant shrinkage than that with 20% SA. Based on these results, a gelatin/starch/SA bioink with 20% SA was selected for the 3D printing of capsular structures.

3.3 3D printing of sustained-release capsular structures

We investigated the printability of the compartmentalized capsular structure with the above bioink. The printing temperature was set based on the thermal transition and mechanical properties of the bioink (Fig. 4). The bioink was heated to 45 °C in the container, the nozzle tip was at 35 °C, and the deposition platform was set to room temperature. By doing this, gelatin formed an aqueous solution at a high temperature of 45 °C, and therefore the bioink exhibited a sol state in the container (Figs. 3a and 3b). The bioink underwent shear through the nozzle (Fig. 3b). Because of the shear-thinning property of the bioink (Fig. 4a), its viscosity

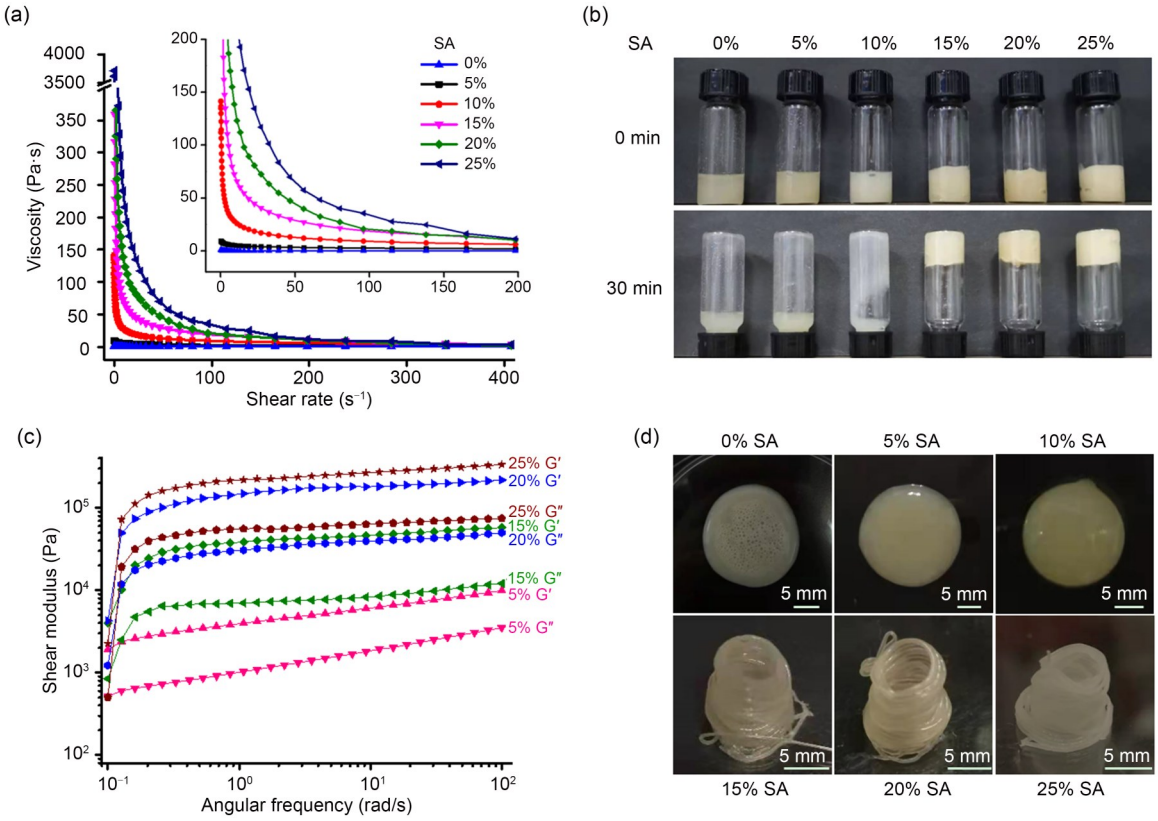

Fig. 4 Characterization of the rheological properties and printability of bioinks. (a) Viscosity-shear rate of bioinks with different SA concentrations. The insert shows the zoom-in region with a smaller shear rate. (b) Flow behavior of different bioinks. (c) Shear moduli of the bioinks in angular frequency sweep mode. G' is the storage modulus, and G" is the loss modulus. (d) Images of 3D structures printed with different bioinks. SA, sodium alginate; 3D, three-dimensional.

decreased, facilitating extrusion through the nozzle (Fig. 3b) to form filaments upon the release of shear stress (Fig. S1d). After deposition on the platform at room temperature, the printed filaments rapidly converted to a gel state (Fig. 3c) because of the sol–gel transition of the gelatin component at room temperature (Duconseille et al., 2015) as well as the superior storage modulus over the loss modulus of the bioinks at room temperature (Fig. 4c). The printed filaments further fused and adhered together, and a 3D capsular structure was printed layer-by-layer by stacking of the filaments (Fig. 3c). During the printing process, different formulations of drugs, such as different colored dyes or the fluorescence tracer DRX, were loaded into different compartments of the capsular device (Fig. 3d).

3.4 Characterization of the compartmentalized capsules

The as-printed capsules had a cream color due to the color of the gelatin component. They exhibited a uniform cone structure as designed, with a visible printing path among the different layers (Figs. 5a and 5b), and the overall sizes approached the designed sizes (Table 2). After drying, the overall dimensions of the capsule decreased, resulting in a solid and compact structure (Figs. 5c and 5d). Compared to the designed parameters, the base diameter decreased from 20.00 mm to (14.30±0.02) mm, and the height decreased from 8.00 mm to (5.80±0.02) mm (Table 2), representing a shrinkage of 28.5% in the base diameter and 27.5% in height.

According to the optical images, the external surface of the capsules showed ridges due to the round shape of the printed filaments (Fig. 5c). However, SEM images revealed that these filaments contacted firmly and fused together between the printed layers (Figs. 5e–5h), forming a compact structure without apparent defects on the external walls or internal divisions (Figs. 5e–5h). Moreover, the porosity of the printed structures was calculated to be only (0.55±0.17)% according to cross-sectional SEM images.

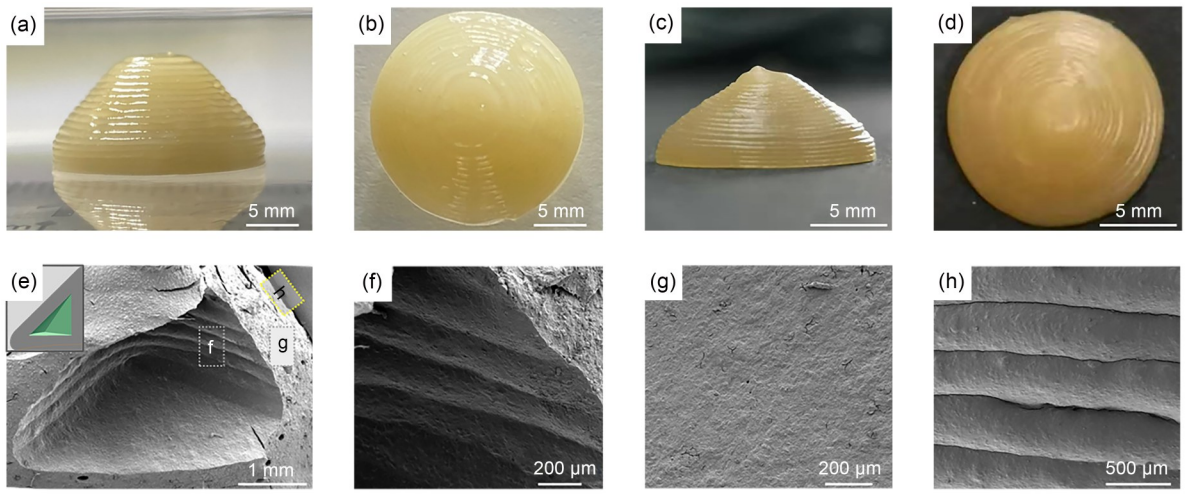

Fig. 5 Morphological characterization of manufactured capsules. (a, b) Front view (a) and top view (b) of as-printed capsule. (c, d) Front view (c) and top view (d) of dehydrated capsule. (e) SEM image of printed capsules. The top-left insert shows the position of the SEM image. (f–h) Zoom-in regions of the SEM image in (e), consisting of an internal wall (f), cross-section (g), and external wall (h) of the printed capsule. SEM, scanning electron microscopy.

Table 2 Comparison of designed and measured parameters of printed capsules

Group	Base diameter (mm)	Height (mm)	External wall thickness (mm)			
			Chamber 1	Chamber 2	Chamber 3	Chamber 4
Designed	20.00	8.00	1.15	1.40	1.65	1.90
As-printed	20.60±0.21	8.80±0.02				
Dried	14.30±0.02	5.80±0.02	0.92±0.09	1.24±0.14	1.33±0.13	1.46±0.08

Data (except for the designed group) are expressed as mean±standard deviation (n=5).

Non-destructive testing by CT scanning revealed that the printed capsule enclosed four individual compartmentalized chambers as designed. The internal divisions separated the compartments, and the external walls enclosed the compartments from the outside (Figs. 6a and 6b). The external wall thickness of the four compartments differed, and encapsulated different sized internal cavities (Figs. 6c–6f). The thickness of the external walls of the four compartments gradually increased from 0.92 to 1.24, 1.33, and 1.46 mm, respectively (Table 2); and the thickness of internal divisions from 1.81 to 2.38, 2.47, and 2.66 mm, respectively. The compartments with thicker external walls enclosed a smaller internal volume (Figs. 6e and 6f). Compared to designed parameters, the obtained structures showed variability and deviation in dimensions, external wall thickness, and internal division thickness (Table 2), resulting in different internal cavity volumes (Figs. 6 and S3). This could be attributed to the precision of the printing (Zhu et al., 2021), superposition and partial fusion between printed layers (Zhu et al., 2021), and shrinkage during the dehydration process. However, the variability of the wall thickness

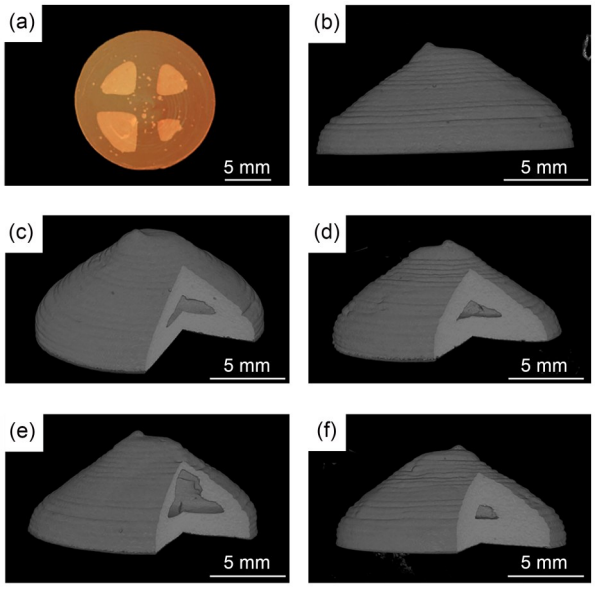

Fig. 6 Characterization of the internal structures of the printed capsules by CT imaging. (a) 3D reconstruction of CT images of a capsule. Dark field represents the framework, and light field represents a cavity in the capsule. (b) Front view of CT images of capsule. (c–f) Cutaway views of four compartments of capsules. CT, computed tomography; 3D, three-dimensional.

was consistent with our structural design (Table 2). The successive increase of external wall thickness of the four compartments made sustained drug release possible through the successive dissolution of the external walls.

3.5 In vitro swelling

For better visualization of in vitro swelling, we printed different colored dyes into the four compartments of the capsules. The printed capsular devices were confirmed as being firmly sealed, as no dye was detected before the drug release assay (Fig. 7, 0 min). The morphological changes and opening behavior of different compartments of the capsules were evaluated in saline solution at 37 °C, and the degradation process of the printed capsules was confirmed by observation of the release of different colored dyes from the capsules (Fig. 7).

The external wall of the first compartment, which was the thinnest, started to dissolve at about 90 min, and had completely dissolved by 120 min, revealing the encapsulated black dye (Fig. 7). The other compartments with thicker external walls concealed the loaded dyes inside the relevant cavities for longer time. Leakage of relevant loaded dyes took place successively from the second, third, and fourth compartments at about 120, 180, and 210 min, respectively, and these compartments completely dissolved at about 150, 210, and 220 min, respectively. Therefore, the effect of the external wall thickness of the capsules on drug release performance was successfully demonstrated.

When immersed in solution at body temperature of 37 °C, gelatin dissolves and degrades as a colloidal solution (Duconseille et al., 2015), starch dissolves (Elvira et al., 2002), and alginate swells. As a result, upon incubation in saline at 37 °C, the printed gelatin/starch/alginate capsules swelled and gradually dissolved, permitting successive drug release from the capsules. However, the opening behavior of each compartment of the capsule was dependent only on the relevant wall thickness (Fig. 7).

3.6 In vitro drug release

We evaluated the drug release profile of the printed capsules using a drug tracer of DXR loaded into the capsule. After immersion in saline, the external walls swelled (Fig. 7), resulting in relatively permeable external walls. Therefore, a small amount of loaded drug slowly permeated through the external walls and diffused into the saline solution. When the external walls of the compartments opened with complete dissolution (Fig.7), the encapsulated drug in each compartment was rapidly released, resulting in a burst in the drug release profiles (Fig. 8).

For capsules with uniform external wall thickness, the four compartments dissolved or degraded from all sides of the capsules simultaneously, resulting in a burst release of encapsulated content from the four compartments simultaneously, therefore showing a single concentrated pulse in the drug release profile (Fig. 8). Moreover, the larger the thickness of the external walls, the more delayed the commencement of delivery (Fig. 8), with $t_{5\%}$ of about 193.3 min for 1.15-μm-thick capsules, and about 317.5 min for 1.90-μm-thick capsules (Table 3). The total drug release duration of capsules with 1.15-μm-thick and 1.90-μm-thick walls lasted for about 267.5 min and 335.0 min, respectively (Table 3).

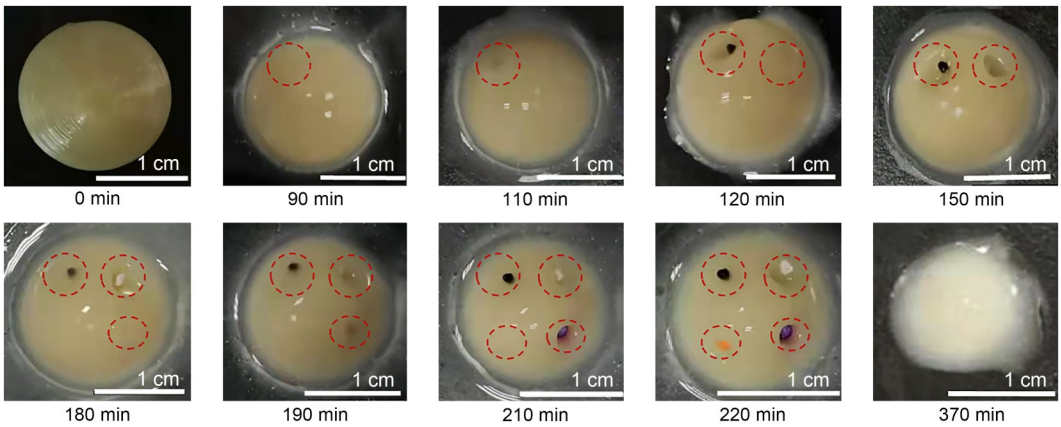

Fig. 7 Images of swelling of printed capsules after incubation in saline for different time points.

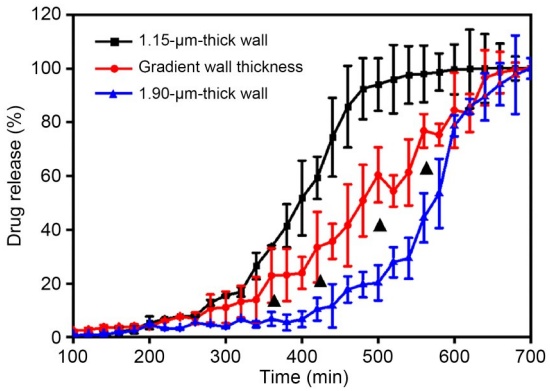

Fig. 8 In vitro drug release profiles of the printed capsules. Black triangles indicate the pulse releases from different compartments of a capsule with a wall thickness gradient.

Table 3 Summary of in vitro drug release

Capsule	$t_{5\%}$ (min)	$t_{95\%-5\%}$ (min)
1.15-μm-thick wall	193.3±5.8	267.5±17.1
Gradient wall thickness	203.8±16.0	410.5±21.6
1.90-μm-thick wall	317.5±22.2	335.0±7.7

$t_{5\%}$, time to 5% release, which indicated the start of drug release; $t_{95\%}$, time to 95% release, which indicated the almost complete drug release; $t_{95\%-5\%}$, time interval to achieve complete release, which defined the duration of drug release.

For the capsules designed with a wall thickness gradient, the different wall thickness of the capsules allowed variation in the time to dissolve, and the successive opening of the external walls allowed a sequential burst drug release, as indicated by four individual pulses at about 360, 420, 500, and 560 min in the drug release curve, respectively (Fig. 8). With the same amount of drug loading, the capsular structure designed with a wall thickness gradient achieved a slower drug release rate and longer drug release duration than those with uniform external wall thickness (Fig. 8 and Table 3), with a total release duration of about 410 min (Table 3).

In this study, we designed and manufactured a multiple compartmentalized capsule structure for controlled drug release using FDM 3D printing technique, and the effect of the bioinspired structure on controlled drug release behavior was successfully demonstrated. The variations in geometry and wall thickness were key issues of the resolution achievable for printing the smallest chambers, and being able to load the ingredients within. As demonstrated, the microgeometry of the compartmentalized structures had a significant effect on the drug release profiles. After being placed in the required environment, a drug can be sustainably released after swelling and degradation of the capsular structures, avoiding the "peak and valley" phenomenon, and keeping the drug concentration within the effective concentration range for a long time.

This work provided an opportunity for personalized and customized medicine with 3D printing of biomimetic capsules for patient-oriented needs. Application of such 3D-printed capsules may enable personalized medicine and drug delivery kinetics as per patient requirements and schedules. The modulation of the wall thickness and the number of compartments may have a substantial influence in guiding the release kinetics of drugs using customized capsules, thereby reducing the number of drug intakes, increasing drug bioavailability, and initiating a sequential and sustained release of desired drugs at a desired time interval. The multiple compartmentalization can also serve to add to the feature of multiple modal therapy in one shot, which therefore could greatly improve patient compliance, cost performance, and therapeutic time. Furthermore, the design aspects of the capsule allow for triggered and digitalized release of the contents of choice to specific needs of patients. Multiple combinational therapies at a customized level are therefore achievable.

As a further development, the capsular device can be modulated to achieve personalized medicine for specific patients. For example, by adjusting the capsular structure design (including variable sizes, more compartments, and more precise wall thicknesses) or drug loading strategies (such as one single drug, multiple drug combinations, and different dosages in one or more of the available compartments), our design has potential to provide more flexible and personal drug delivery requirements, to improve personalized and precise medicine. The printed capsular structures can also be used for the delivery of pharmaceuticals, biologics, nutraceuticals, minerals, or food extracts, individually or in combination. Moreover, compared to the relatively rapid degradation/dissolution of biomaterials used in the present study, other biodegradable materials with a slower degradation rate, such as poly(lactic acid) (PLA) (Carlier et al., 2019) and poly(ε-caprolactone) (PCL) (Holländer et al., 2016), can be fabricated with a similar design, allowing extended drug release for weeks or months.

4 Conclusions

Inspired by natural plant structures, we designed a multiple compartmentalized capsular structure, and successfully manufactured capsules using FDM 3D printing to achieve controlled drug release. Bioinks of gelatin, starch, and alginate were regulated to ensure good printability and shape fidelity of the capsular structures. The rapid prototyping ability of FDM was highly advantageous in the printing of the capsular design. Through assembly of four compartments with different geometries and drug formulations, this capsular device was able to achieve successive drug release pulses, and allowed a sustained drug release for a total duration of 410 min. This bio-designed and manufactured structure would enable real-time adjustment of the number of compartments and their wall characteristics, and meet different patient needs, therefore improving the extent of personalized medicine of drug therapy.

Acknowledgments

This work was supported by the National Key Research and Development Program of China (No. 2018YFB1105100), the National Natural Science Foundation of China (No. 81871484), and the Start-up Funding of Wuhan University (No. 20035), China.

Author contributions

Jingwen LI and Mingxin WU designed the study, and collected the data. Wenhui CHEN performed the CT imaging and analysis. Haiyang LIU assisted the 3D printing. Di TAN helped with the statistical analyses. Shengnan SHEN contributed to the discussion. Yifeng LEI guided the study, wrote and revised the manuscript. Longjian XUE organized and supervised the project. All authors have read and approved the final manuscript, and therefore, have full access to all the data in the study and take responsibility for the integrity and security of the data.

Compliance with ethics guidelines

Jingwen LI, Mingxin WU, Wenhui CHEN, Haiyang LIU, Di TAN, Shengnan SHEN, Yifeng LEI, and Longjian XUE declare that they have no conflicts of interests.

This article does not contain any studies with human or animal subjects performed by any of the authors.

References

An G, Guo FX, Liu XM, et al., 2020. Functional reconstruction of injured corpus cavernosa using 3D-printed hydrogel scaffolds seeded with HIF-1α-expressing stem cells. *Nat Commun*, 11:2687. https://doi.org/10.1038/s41467-020-16192-x

Bohidar HB, Jena SS, 1993. Kinetics of sol−gel transition in thermoreversible gelation of gelatin. *J Chem Phys*, 98(11): 8970-8977. https://doi.org/10.1063/1.464456

Bose S, Ke DX, Sahasrabudhe H, et al., 2018. Additive manufacturing of biomaterials. *Prog Mater Sci*, 93:45-111. https://doi.org/10.1016/j.pmatsci.2017.08.003

Carlier E, Marquette S, Peerboom C, et al., 2019. Investigation of the parameters used in fused deposition modeling of poly(lactic acid) to optimize 3D printing sessions. *Int J Pharm*, 565:367-377. https://doi.org/10.1016/j.ijpharm.2019.05.008

Chen G, Xu YH, Kwok PCL, et al., 2020. Pharmaceutical applications of 3D printing. *Addit Manuf*, 34:101209. https://doi.org/10.1016/j.addma.2020.101209

Duconseille A, Astruc T, Quintana N, et al., 2015. Gelatin structure and composition linked to hard capsule dissolution: a review. *Food Hydrocoll*, 43:360-376. https://doi.org/10.1016/j.foodhyd.2014.06.006

Economidou SN, Uddin MJ, Marques MJ, et al., 2021. A novel 3D printed hollow microneedle microelectromechanical system for controlled, personalized transdermal drug delivery. *Addit Manuf*, 38:101815. https://doi.org/10.1016/j.addma.2020.101815

Elvira C, Mano JF, Roman JS, et al., 2002. Starch-based biodegradable hydrogels with potential biomedical applications as drug delivery systems. *Biomaterials*, 23(9): 1955-1966. https://doi.org/10.1016/s0142-9612(01)00322-2

Fina F, Goyanes A, Madla CM, et al., 2018. 3D printing of drug-loaded gyroid lattices using selective laser sintering. *Int J Pharm*, 547(1-2):44-52. https://doi.org/10.1016/j.ijpharm.2018.05.044

Gioumouxouzis CI, Karavasili C, Fatouros DG, 2019. Recent advances in pharmaceutical dosage forms and devices using additive manufacturing technologies. *Drug Discov Today*, 24(2):636-643. https://doi.org/10.1016/j.drudis.2018.11.019

Guvendiren M, Lu HD, Burdick JA, 2012. Shear-thinning hydrogels for biomedical applications. *Soft Matter*, 8(2): 260-272. https://doi.org/10.1039/c1sm06513k

Holland I, Logan J, Shi JZ, et al., 2018. 3D biofabrication for tubular tissue engineering. *Bio-Des Manuf*, 1(2):89-100. https://doi.org/10.1007/s42242-018-0013-2

Holländer J, Genina N, Jukarainen H, et al., 2016. Three-dimensional printed PCL-based implantable prototypes of medical devices for controlled drug delivery. *J Pharm Sci*, 105(9):2665-2676. https://doi.org/10.1016/j.xphs.2015.12.012

Isreb A, Baj K, Wojsz M, et al., 2019. 3D printed oral theophylline doses with innovative 'radiator-like' design: impact of polyethylene oxide (PEO) molecular weight. *Int J Pharm*, 564:98-105.

https://doi.org/10.1016/j.ijpharm.2019.04.017

Jameson JL, Longo DL, 2015. Precision medicine-personalized, problematic, and promising. *N Engl J Med*, 372(23): 2229-2234. https://doi.org/10.1056/NEJMsb1503104

Kadry H, Al-Hilal TA, Keshavarz A, et al., 2018. Multi-purposable filaments of HPMC for 3D printing of medications with tailored drug release and timed-absorption. *Int J Pharm*, 544(1):285-296. https://doi.org/10.1016/j.ijpharm.2018.04.010

Kyobula M, Adedeji A, Alexander MR, et al., 2017. 3D inkjet printing of tablets exploiting bespoke complex geometries for controlled and tuneable drug release. *J Control Release*, 261:207-215. https://doi.org/10.1016/j.jconrel.2017.06.025

Lawlor KT, Vanslambrouck JM, Higgins JW, et al., 2021. Cellular extrusion bioprinting improves kidney organoid reproducibility and conformation. *Nat Mater*, 20(2):260-271. https://doi.org/10.1038/s41563-020-00853-9

Lee KY, Mooney DJ, 2012. Alginate: properties and biomedical applications. *Prog Polym Sci*, 37(1):106-126. https://doi.org/10.1016/j.progpolymsci.2011.06.003

Li QJ, Guan XY, Cui MS, et al., 2018. Preparation and investigation of novel gastro-floating tablets with 3D extrusion-based printing. *Int J Pharm*, 535(1-2):325-332. https://doi.org/10.1016/j.ijpharm.2017.10.037

Li XR, Deng QF, Zhuang TT, et al., 2020. 3D bioprinted breast tumor model for structure—activity relationship study. *Bio-Des Manuf*, 3(4):361-372. https://doi.org/10.1007/s42242-020-00085-5

Li XY, Wu MB, Xiao M, et al., 2019. Microencapsulated β-carotene preparation using different drying treatments. *J Zhejiang Univ-Sci B (Biomed & Biotechnol)*, 20(11): 901-909. https://doi.org/10.1631/jzus.B1900157

Liaw CY, Guvendiren M, 2017. Current and emerging applications of 3D printing in medicine. *Biofabrication*, 9(2):024102. https://doi.org/10.1088/1758-5090/aa7279

Ligon SC, Liska R, Stampfl J, et al., 2017. Polymers for 3D printing and customized additive manufacturing. *Chem Rev*, 117(15):10212-10290. https://doi.org/10.1021/acs.chemrev.7b00074

Lim SH, Chia SMY, Kang LF, et al., 2016. Three-dimensional printing of carbamazepine sustained-release scaffold. *J Pharm Sci*, 105(7):2155-2163. https://doi.org/10.1016/j.xphs.2016.04.031

Lim SH, Kathuria H, Tan JJY, et al., 2018. 3D printed drug delivery and testing systems—a passing fad or the future? *Adv Drug Deliv Rev*, 132:139-168. https://doi.org/10.1016/j.addr.2018.05.006

Maharjan S, Bonilla D, Sindurakar P, et al., 2021. 3D human nonalcoholic hepatic steatosis and fibrosis models. *Bio-Des Manuf*, 4(2):157-170. https://doi.org/10.1007/s42242-020-00121-4

Maroni A, Melocchi A, Parietti F, et al., 2017. 3D printed multi-compartment capsular devices for two-pulse oral drug delivery. *J Control Release*, 268:10-18. https://doi.org/10.1016/j.jconrel.2017.10.008

Noor N, Shapira A, Edri R, et al., 2019. 3D printing of personalized thick and perfusable cardiac patches and hearts. *Adv Sci*, 6(11):1900344. https://doi.org/10.1002/advs.201900344

Norman J, Madurawe RD, Moore CMV, et al., 2017. A new chapter in pharmaceutical manufacturing: 3D-printed drug products. *Adv Drug Deliv Rev*, 108:39-50. https://doi.org/10.1016/j.addr.2016.03.001

Ozbolat IT, Hospodiuk M, 2016. Current advances and future perspectives in extrusion-based bioprinting. *Biomaterials*, 76:321-343. https://doi.org/10.1016/j.biomaterials.2015.10.076

Ozbolat IT, Peng WJ, Ozbolat V, 2016. Application areas of 3D bioprinting. *Drug Discov Today*, 21(8):1257-1271. https://doi.org/10.1016/j.drudis.2016.04.006

Paxton N, Smolan W, Bock T, et al., 2017. Proposal to assess printability of bioinks for extrusion-based bioprinting and evaluation of rheological properties governing bioprintability. *Biofabrication*, 9(4):044107. https://doi.org/10.1088/1758-5090/aa8dd8

Peng WM, Liu YF, Jiang XF, et al., 2019. Bionic mechanical design and 3D printing of novel porous Ti6Al4V implants for biomedical applications. *J Zhejiang Univ-Sci B (Biomed & Biotechnol)*, 20(8):647-659. https://doi.org/10.1631/jzus.B1800622

Pereira BC, Isreb A, Forbes RT, et al., 2019. 'Temporary plasticiser': a novel solution to fabricate 3D printed patient-centred cardiovascular 'polypill' architectures. *Eur J Pharm Biopharm*, 135:94-103. https://doi.org/10.1016/j.ejpb.2018.12.009

Placone JK, Engler AJ, 2018. Recent advances in extrusion-based 3D printing for biomedical applications. *Adv Healthc Mater*, 7(8):1701161. https://doi.org/10.1002/adhm.201701161

Rastogi P, Kandasubramanian B, 2019. Review of alginate-based hydrogel bioprinting for application in tissue engineering. *Biofabrication*, 11(4):042001. https://doi.org/10.1088/1758-5090/ab331e

Trivedi M, Jee J, Silva S, et al., 2018. Additive manufacturing of pharmaceuticals for precision medicine applications: a review of the promises and perils in implementation. *Addit Manuf*, 23:319-328. https://doi.org/10.1016/j.addma.2018.07.004

Urciuolo A, Poli I, Brandolino L, et al., 2020. Intravital three-dimensional bioprinting. *Nat Biomed Eng*, 4(9):901-915. https://doi.org/10.1038/s41551-020-0568-z

Velasco-Hogan A, Xu J, Meyers MA, 2018. Additive manufacturing as a method to design and optimize bioinspired structures. *Adv Mater*, 30(52):1800940. https://doi.org/10.1002/adma.201800940

Wu MX, Zhang YJ, Huang H, et al., 2020. Assisted 3D

printing of microneedle patches for minimally invasive glucose control in diabetes. *Mater Sci Eng C*, 117:111299. https://doi.org/10.1016/j.msec.2020.111299

You F, Wu X, Kelly M, et al., 2020. Bioprinting and *in vitro* characterization of alginate dialdehyde—gelatin hydrogel bio-ink. *Bio-Des Manuf*, 3(1):48-59. https://doi.org/10.1007/s42242-020-00058-8

Zhang B, Xue Q, Hu HY, et al., 2019. Integrated 3D bioprinting-based geometry-control strategy for fabricating corneal substitutes. *J Zhejiang Univ-Sci B (Biomed & Biotechnol)*, 20(12):945-959. https://doi.org/10.1631/jzus.B1900190

Zhang BQ, Sun H, Wu LN, et al., 2019. 3D printing of calcium phosphate bioceramic with tailored biodegradation rate for skull bone tissue reconstruction. *Bio-Des Manuf*, 2(3):161-171. https://doi.org/10.1007/s42242-019-00046-7

Zhang HB, Jackson JK, Chiao M, 2017. Microfabricated drug delivery devices: design, fabrication, and applications. *Adv Funct Mater*, 27(45):1703606. https://doi.org/10.1002/adfm.201703606

Zhang NZ, Liu HS, Yu L, et al., 2013. Developing gelatin-starch blends for use as capsule materials. *Carbohydr Polym*, 92(1):455-461. https://doi.org/10.1016/j.carbpol.2012.09.048

Zhu YZ, Joralmon D, Shan WT, et al., 2021. 3D printing biomimetic materials and structures for biomedical applications. *Bio-Des Manuf*, 4(2):405-428. https://doi.org/10.1007/s42242-020-00117-0

Supplementary information

Figs. S1–S3